Journal of Naval Architecture and Marine Engineering
January, 2025
https://doi.org/10.3329/jname.v22i1.77636 *http://www.banglajol.info*

AUGMENTING THERMAL-MATERIAL TRANSPORT IN BOUNDARY-LAYER FLOW OVER AN UPRIGHT SHEET: AN EXPLICIT FINITE DIFFERENCE APPROACH

Mohammed Jahir Uddin[1], R. Nasrin[1*], and Eid S. Alatawi[2]
[1]Department of Mathematics, Bangladesh University of Engineering and Technology, Dhaka-1000, Bangladesh
[2]Department of Mechanical Engineering, Faculty of Engineering, University of Tabuk, Tabuk, 71491, Saudi Arabia
*Correspondence: rehena@math.buet.ac.bd

Abstract:

Transporting heat and mass in boundary-layer flows is crucial for various industries, including petroleum and agricultural engineering, gas turbines, nuclear power facilities, heat exchangers, cooling systems, and chemical processing. Understanding these processes is essential for advancing scientific knowledge and improving practical engineering applications across multiple fields. This study aims to investigate the effects of thermal and solute buoyancy forces on the fluctuating flow within a boundary layer over an upright permeable flat sheet with heat generation. This analysis requires modifying the nonlinear and time-varying partial differential equations (PDEs) to address the continuity, momentum, energy, and concentration balance equations. After developing a mathematical model, the explicit finite difference method (EFDM) is utilized to solve a set of nonlinear dimensionless partial differential equations and suitable boundary conditions (BCs). The EFDM technique is described step-by-step and tailored to the specific analyzed model. The stability, convergence, finding a suitable uniform meshing, steady-state condition, and code validation are conducted. This study investigates the distributions of velocity, temperature, and concentration influenced by physical forces, specifically buoyancy and heat generation. It provides a detailed analysis of the mean and local rates of the skin friction coefficient and heat and material transport. The findings demonstrate that fluid velocity rises as buoyancy increases, and increasing heat generation increases heat-mass heat transmission rates. The practical behavior results from the pressure gradient caused by thermal buoyancy force. Two novel linear regression equations with multiple variables are derived from the outputs. This study establishes a robust and adaptable framework to enhance understanding of boundary-layer flows across various practical applications. It leverages advanced modeling techniques, incorporates variable properties, employs unsteady analysis, considers surface porosity, and investigates the effects of heat generation and thermal-solutal buoyancy forces.

Keywords: Thermal-material transport, boundary-layer flow, unsteady porous medium, heat generation, EFDM

NOMENCLATURE

B (JT^{-1})	magnetic field intensity	α (m^2s^{-1})	thermal diffusivity
D_m(m^2s^{-1})	coefficient of mass diffusivity	β (K^{-1})	coefficient of volumetric expansion
Gr	thermal Grashof number	β^*(K^{-1})	volumetric expansion coefficient with concentration
Gm	solutal Grashof number		
Ha	Hartmann number	η	similarity variable
J (Am^{-1})	current density vector	κ($JA^{-2}m^{-1}$)	permeability
k ($Wm^{-1}K^{-1}$)	thermal conductivity	κ_0	Roseland means absorption coefficient
q (ms^{-1})	velocity vector		
U_0 (ms^{-1})	constant velocity	μ ($kgm^{-1}s^{-1}$)	coefficient of viscosity
u (ms^{-1})	velocity component along the x-axis	φ	dissipation function involving the viscous stress

Greek symbols

 Received on: Nov., 2024

1. Introduction

Magnetohydrodynamics (MHD) is an integral part of physics, studying the contact of electrically accompanying fluids with magnetic fields through electromagnetism. It has uses across various fields such as geophysics, astrophysics, and solar physics. Earthquakes, stellar and planetary magnetospheres engineering (such as liquid-metal, polymer engineering, and plasma confinement), biomedical engineering, and the textile industry. The numerous applications of the MHD stream in a porous material have fascinated the curiosity of many researchers.

Detailed discussions of this research can be accessed through (Ajay and Srinivasa, 2021, Ahmed et al. 2018, Arifuzzaman et al. 2018, Das et al. 2016, Samiulhaq et al. 2014, Krishna et al. 2019, Ge-JiLe et al. 2021, Yun-Jie et al. 2021). Many scientific and technical disciplines, including filtration mechanics, rock mechanics, soil mechanics, geology, biology, metal forming, and others, use porous media. Energy recovery, geothermal central heating, thermal energy storage, oil extraction, filtering device flow, and natural environment evacuation all use thermal convection. The design of chemical processing equipment, thermal energy storage, and nuclear power plants relies on the simultaneous thermal and material transmission phenomenon in a fluid media. Makinde and Aziz (2010), investigated the phenomenon of combined convection in MHD from an upright plate immersed in a porous material. The study specifically examined the effects of convective boundary circumstances on this process. Reddy et al. (2009) investigated the unsteady magnetohydrodynamic convection flow phenomenon. The research investigation addressed the fluid dynamics in a semi-infinite upright permeable moving plate. The study specifically examined the impact of mass transfer and variations in viscosity and thermal conductivity. Ali et al. (2017) revealed a comprehensive examination of the mathematical modeling of the movement of mass and heat through a stretched wedge surface. The pivotal emphasis of the author's work revolved around the analysis of dimensionless parameters associated with the velocity, temperature, and concentration aspects of nanoparticle fields. Tarammim et al. (2020) studied the characteristics of two-dimensional shapes and unstable magnetohydrodynamic free convection streams across upright plates. The researchers used the EFDM to find the solution and assess stability. However, they did not investigate the concentration distribution.

Alam et al. (2006) examined the phenomenon of joint free-forced convective and mass transfer across an upright permeable plate. The researchers investigated many factors, such as heat production and thermal diffusion. Jahir and Nasrin (2022) examine the effect of radiation and heat production on the magneto-convective fluid movement across a vertically oriented porous plate. Additionally, they analyzed stable and unstable conditions. Ullah et al. (2021) investigated the phenomenon of two-dimensional unsteady magnetohydrodynamic convective heat transfer across an upright plate, considering the impact of radiation. They use the FDM, established stability, and convergence analysis but do not work on material profiles. Islam et al. (2022) investigated the mathematical modeling of unstable flow in a half-moon-shaped area. The researchers considered the effects of uniform and non-uniform temperature and electromagnetic magnitude. Alam et al. (2013) scrutinized the movement of thermal and material occurring in a magnetohydrodynamic convection-free flow across an inclined plate. They specifically took into consideration the influence of a Hall current. Abdullaameed et al. (2013) demonstrated closed-form approaches for unstable MHD streams in a porous material with barrier evaporation. Shamshuddin et al. (2022) examined radiative thermal energy on a nanoliquid of the Casson type produced by a rapidly heated porous material with Brownian motion and thermophoresis impacts. Mosharrof et al. (2022) exposed radiation impacts the time-varying of the MHD thermal-material transport using micro polar binary conjunction.

Sohail et al. (2022) and Nasrin et al. (2024) solved governing equations nanofluid flow by finite element technique where specifically Sohail et al. (2022) used Pseudo-plastic liquid-based ternary hybrid nanofluid through a permeable stretching sheet, and Nasrin et al. (2024) used water-propylene glycol based nanofluid inside an interconnected domain to enhance thermal performance. Alqahtani et al. (2024), Khan et al. (2024), and Zeeshan et al. (2023a, 2023b) numerically investigated the heat-mass transport, velocity-thermal slips effects at the boundary enclosing energy perspective, variable magnetic field, thermal conductivity, heat source, nonlinear thermal radiation, etc. They used two-dimensional governing equations for Williamson nanofluid, hybrid nanofluid, Buongionro nanofluid model through stretching/shrinking sheet, and permeable wedge sheet. Their research showed the heat and mass transport phenomena.

Based on the existing literature, it can be inferred that our study investigates the time-varying convective thermal-material conveyance through an upright porous plate, considering the impact of thermal and solutal

buoyancy forces and heat production. According to the literature review conducted, it is recommended that scientists need to continue focusing their attention on the following areas of study:

- Research conducted to justify the experimentally demonstrated parameters is necessary.
- Choosing the ideal mesh size significantly after several trials with various mesh sizes for the flow model inside the boundary layer (BL) is rare.
- A few studies focus on multiple (nine) parameters and dimensionless numbers that affect heat transfer performance in conjunction with employing an upright porous plate.
- Continuous parameter values are tested continuously for the steady-state situation in the flow model that has not yet been worked.
- The flow procedure's geometry has attracted considerable attention, but more work is required to identify which form would best enable heat and mass transfer.

Motivated by the increasing application of free convection flow in various engineering and industrial processes and the significance of radiative heat transfer in thermal and buoyancy force problems and their applications, this paper focuses on examining the computational approaches for analyzing the convective thermal and material fluid flow around an upright porous plate.
This research examines the following aspects:

- ❖ Scrutinize the system of governing equations of Newtonian-laminar-incompressible flow, satisfying the Boussinesq approximation and heat-mass transfer based on the considered geometry.
- ❖ Analyze the impact of changing the input parameters on the resulting velocity, thermal, and material fields.
- ❖ Evaluate the consequence of friction factor, thermal transfer efficacy, and the effect of mass transfer rate in engineering curiosity.
- ❖ Investigate the stability and convergence analysis for accurate computations.

The study's significant innovation involves examining the implications of nine critical indeterminate numbers and parameters in conjunction with the porous sheet on thermal and solute buoyancy forces. This analysis has not been previously undertaken. This characteristic sets our present investigation apart from previous ones. The current research centers on identifying critical indeterminate numbers and parameters associated with an unsteady fluid flow over an upright porous sheet influenced by thermal and solutal buoyancy forces. This research holds promise for uncovering new flow dynamics and enhancing various engineering applications. Understanding the interaction between these parameters has the potential to significantly improve control over heat and mass transfer processes, thereby driving advancements across multiple fields.

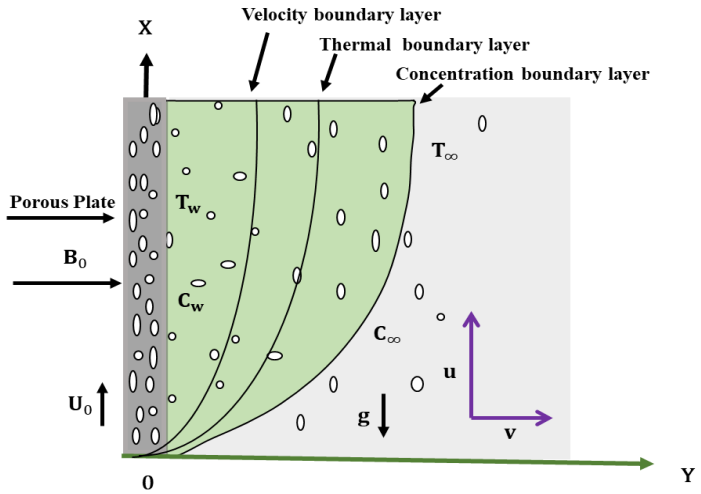

Figure 1: Schematic diagram of the considered model geometry

The governing equations are formulated during the initial phase, and numerical analyses are included. The results and discussions are presented in the second stage, along with graphs, tables, and comparisons. Finally, a summary of the substantial findings of this research is given. Subsequently, significant prospective research and references pertinent to this study are comprised.

2. Schematic Model

The dynamics of MHD-free convection-permitted streams involve fluid that is both viscid and viscoelastic, as well as electrically insulating. These flows occur around an upright sheet situated in a medium with permeability. The x-axis of Figure 1 is directed upwards vertically towards the porous material. Let's assume that the x-axis and y-axis components of velocity are denoted by u and v respectively. Due to the supposition that the surface is in a vertical plane, the flow factors are only based on the typical distances y and t, i.e., U(y, t). These include the flat sheet and the fluid starting at an identical temperature. The upright sheet temperature increases $T_w(>T_\infty)$, and the species concentration is increased simultaneously.

2.1 Physical implications

This research holds significant practical implications for engineering, environmental sciences, and materials processing. Examining thermal-material transport within boundary-layer flows can bring about transformative changes across various fields that demand efficient thermal management and precise material transport. Below are some potential applications and impacts:

- Industrial heat transfer systems
- Aerospace and automotive engineering
- Renewable energy systems
- Materials processing and manufacturing
- Environmental applications
- Advancements in numerical methods

2.2 Assumptions

All norms and estimates for the typical stream are taken from (Alam et al. 2006, Ali et al. 2017, Tarammim et al. 2020, Ullah et al. 2021, Jahir and Nasrin, 2022) and as follows:

- ❖ The flat surface is typically subjected to a consistent magnetic field.
- ❖ The actual transverse magnetic field strength and magnetic Reynolds number are significant.
- ❖ The flow is laminar and has constant density.
- ❖ The permeable sheet induces the flow within the material.
- ❖ The effects of radiant heat and buoyancy forces can be observed individually in the energy and momentum equations.
- ❖ According to the Roseland (1936) approximation of radiative heat flux, the accurate prediction of thermal emission can be achieved by employing Taylor series development.

3. Mathematical Model

The asymptotic boundary conditions are imposed throughout the computational domain. Exhausting the assumptions above, Boussinesq's approach and the research of (Ali et al. 2021, Nasrin and Alim, 2009a, 2009b), the governing equations in vector form of the current analysis are as follows:

$$\nabla.\mathbf{q} = 0 \tag{1}$$

$$\frac{\partial q}{\partial t} + (\mathbf{q}.\nabla)\mathbf{q} = \mathbf{F} - \frac{1}{\rho}\nabla P + \upsilon\nabla^2\mathbf{q} - \frac{\nu}{k}\mathbf{q} + \frac{1}{\rho}(\mathbf{J}\times\mathbf{B}) \tag{2}$$

$$\frac{\partial T}{\partial t} + (\mathbf{q}.\nabla)T = \frac{\kappa}{\rho c_p}\nabla^2 T + \frac{\upsilon}{C_p}\phi \tag{3}$$

$$\frac{\partial C}{\partial t} + (\mathbf{q}.\nabla)C = D_m \nabla^2 C \tag{4}$$

Here the velocity vector, $\mathbf{q} = u\mathbf{i} + v\mathbf{j} + w\mathbf{k}$,
the coefficient of kinematic viscosity, $v = \frac{\mu}{\rho}$,
the MHD body force, known as Lorentz force, $\mathbf{J} \times \mathbf{B} = -\sigma {B_0}^2 u$,
the relation among density difference, $\nabla\rho = \rho - \rho_\infty$,
the temperature difference, $\nabla T = T - T_\infty$
the concentration difference, $\nabla C = C - C_\infty$,
the dissipation function involving the viscous stress,

$$\phi = 2\left\{\left(\frac{\partial u}{\partial x}\right)^2 + \left(\frac{\partial v}{\partial y}\right)^2 + \left(\frac{\partial w}{\partial z}\right)^2\right\} + \left(\frac{\partial v}{\partial x} + \frac{\partial u}{\partial y}\right)^2 + \left(\frac{\partial w}{\partial y} + \frac{\partial v}{\partial z}\right)^2 + \left(\frac{\partial u}{\partial z} + \frac{\partial w}{\partial x}\right)^2$$

the term $\frac{\rho-\rho_\infty}{\rho} = -\beta(\mathrm{T} - \mathrm{T}_\infty) - \beta^*(\mathrm{C} - \mathrm{C}_\infty)$,
and the term $F_x - \frac{1}{\rho}\frac{\partial p}{\partial x} = g\beta(T - T_\infty) + g\beta^*(C - C_\infty)$.

Considering internal thermal radiation and heat generation, we can generate the two-dimensional time-dependent continuity, momentum, energy, and concentration equations of the fluid as follows:

$$\frac{\partial u}{\partial x} + \frac{\partial v}{\partial y} = 0 \tag{5}$$

$$\frac{\partial u}{\partial t} + u\frac{\partial u}{\partial x} + v\frac{\partial u}{\partial y} = \nu\frac{\partial^2 u}{\partial y^2} + g\beta(\mathrm{T} - \mathrm{T}_\infty) + g\beta^*(\mathrm{C} - \mathrm{C}_\infty) - \frac{\sigma \mathrm{B}_0^2}{\rho}u - \frac{\nu}{\kappa}u \tag{6}$$

$$\frac{\partial T}{\partial t} + u\frac{\partial T}{\partial x} + v\frac{\partial T}{\partial y} = \frac{\kappa}{\rho C_p}\frac{\partial^2 T}{\partial y^2} + \frac{\upsilon}{C_p}\left(\frac{\partial u}{\partial y}\right)^2 - \frac{1}{\rho C_p}\frac{\partial q_r}{\partial y} + \frac{Q_0}{\rho C_P}(T - T_\infty) \tag{7}$$

$$\frac{\partial \mathrm{C}}{\partial \mathrm{t}} + u\frac{\partial \mathrm{C}}{\partial \mathrm{x}} + v\frac{\partial \mathrm{C}}{\partial \mathrm{y}} = D_m\frac{\partial^2 \mathrm{C}}{\partial \mathrm{y}^2} \tag{8}$$

The consistent BCs, reflecting Ali et al. (2016, 2017a, 2017b) are:

$$u = U_0,\ v = 0,\ T = T_w,\ C = C_w \ \ at\ y = 0$$
$$u \to 0,\ T \to T_\infty,\ C \to C_\infty \text{ at } y \to \infty \tag{9}$$

Where B_0 represents the constant magnetic field, β signifies the co-efficient of volumetric enlargement, β^* represents the co-efficient of extension with concentration, ρ is the fluid density, C_p is the specific heat, H means the temperature discharge for each unit material, and U_0 represents the fluid's homogenous velocity. At the same time, the remaining symbols hold their conventional implications.

Following conventional alterations leads to forming a non-dimensional PDE method with BCs [Nazeer et al. (2021a, 2021b)]:

$$u = U_0 U,\ v = VU_0,\ Y = \frac{yU_0}{\nu},\ X = \frac{xU_0}{\nu},\ \eta = \frac{tU_0^2}{\nu}, T = T_\infty + (T_w - T_\infty)\bar{T},\ \ C = C_\infty + (C_w - C_\infty)\bar{C}$$

Equations (5), (6), (7), and (8), reliable BCs (9), and exact calculations provide the subsequent nonlinear dimensionless differential equations like Hossain et al. (2023), Ali et al. (2023), Uddin and Nasrin (2023)

$$\frac{\partial U}{\partial X} + \frac{\partial V}{\partial Y} = 0 \tag{10}$$

$$\frac{\partial U}{\partial \eta} + U\frac{\partial U}{\partial X} + V\frac{\partial U}{\partial Y} = \frac{\partial^2 U}{\partial Y^2} + Gr\bar{\mathrm{T}} + Gm\bar{\mathrm{C}} - MU - NU \tag{11}$$

$$\frac{\partial \bar{\mathrm{T}}}{\partial \eta} + U\frac{\partial \bar{\mathrm{T}}}{\partial X} + V\frac{\partial \bar{\mathrm{T}}}{\partial Y} = \frac{1}{Pr}\frac{\partial^2 \bar{\mathrm{T}}}{\partial Y^2} + Ec\left(\frac{\partial U}{\partial Y}\right)^2 + R\frac{\partial^2 \bar{\mathrm{T}}}{\partial Y^2} + H\bar{\mathrm{T}} \tag{12}$$

$$\frac{\partial \bar{\mathrm{C}}}{\partial \eta} + U\frac{\partial \bar{\mathrm{C}}}{\partial X} + V\frac{\partial \bar{\mathrm{C}}}{\partial Y} = \frac{1}{Sc}\frac{\partial^2 \bar{\mathrm{C}}}{\partial Y^2} \tag{13}$$

The BCs are:

$$U = 1,\ V = 0,\ \bar{T} = 1, \bar{C} = 1\ at\ Y = 0$$
$$U = 0,\ \bar{T} = 0,\ \bar{C} = 0 \text{ at } Y \to \infty \tag{14}$$

According to Nasrin and Alim (2009b), Das et al. (2016), Ajay and Srinivasa (2021), and Uddin and Nasrin (2023), the engineering factors or parameters are Grashof number, $Gr = \frac{\nu\, g\, \beta(\mathrm{T_w} - \mathrm{T_\infty})}{\mathrm{U_0^3}}$, magnetic field, $M = \frac{\sigma\, \nu\, B_0^2}{\rho U_0^2}$,

solutal Grashof number, $Gm = \frac{\nu\, g\, \beta^*(C_w - C_\infty)}{U_0^3}$, porosity, $N = \frac{\nu^2}{\kappa\, U_0^2}$, Prandtl number, $Pr = \frac{\nu}{\alpha}$, Eckert number, $Ec = \frac{U_0^2}{C_p\,(T_w - T_\infty)}$, radiation, $R = \frac{16\sigma^* T_\infty^3}{3\rho\, C_p\, \kappa_0\, (T_w - T_\infty)}$, Schmidt number, $Sc = \frac{\nu}{D_m}$, heat generation, $H = \frac{Q_0\, \nu}{U_0^2 \rho\, C_p}$.

The thermo-physical properties of the fluid (water at 4°C) used in this research are thermal diffusivity 1.43 × 10^{-7} m^2/s, thermal conductivity 0.606 W/m.K, viscosity 10^{-3} Pa.s, density 1000 kg/m^3, specific heat capacity 4179 J/kg.K, and volume expansion coefficient, 2.1×10^{-7} (1/K).

The whole structure of the flow process for the current research is shown in Uddin and Nasrin (2023) with the required coordinates.

3.1 Physical imperative quantities

Physical factors, such as skin friction coefficient and thermal and material transmission rates, are crucial in engineering. These are taken from Hossain et al. (2023), Ali et al. (2023), Uddin and Nasrin (2023), and given as follows:

3.1.1 Skin friction coefficient

It is a substantial dimensionless physical factor in engineering-relevant boundary layer fluxes. The skin friction coefficient typically denotes the shear stress occurring at the boundary of the sheet. It happens when the fluid moves toward the surface of the material going through it. The non-dimensional expression representing the local and average shear stresses in the x-direction at the sheet's surface are:

$\tau_{xL} = \mu_0 \frac{\partial U}{\partial Y}$ and $\tau_{xA} = \mu_0 \int \frac{\partial U}{\partial Y} dX$, respectively. (15)

3.1.2 Heat transfer rate

Regarding the Nusselt number (*Nu*), heat transmission rate refers to the quantity of heat that can be conveyed per unit of time in particular materials. This corporeal substance is calculable at the ends of surfaces and walls. The local and mean Nusselt numbers are:

$Nu_L = -\mu_0 \frac{\partial T}{\partial y}$ and $Nu_A = -\mu_0 \int \frac{\partial \bar{\bar{T}}}{\partial Y} dX$, respectively. (16)

3.1.3 Mass transfer rate

The Sherwood number (*Sh*) is a dimensionless parameter that quantifies the mass transfer rate, essential in various engineering applications. This number is commonly associated with the efficiency of mass transmission. In practice, both local and mean Sherwood numbers are utilized to provide insight into this mass transfer process:

$Sh_L = -\mu_0 \left(\frac{\partial C}{\partial y}\right)$ and $Sh_A = -\mu_0 \int \frac{\partial \bar{C}}{\partial Y} dX$, respectively. (17)

4. Numerical Model

The EFDM can computationally analyze the non-dimensional governing nonlinear PDEs (10-13) with pertinent BCs (14). EFDM is a powerful tool for solving boundary layer flow problems due to its simplicity, low computational overhead, flexibility, and suitability for time-dependent analyses. While careful attention to stability constraints is required, its advantages make it a popular choice in various engineering and scientific applications. The EFDM can convert linear (non-linear) ordinary/partial differential equations (ODE/PDE) and time-independent and dependent complications into a system of linear ODE. To determine the difference equations, the flowing area is separated into a node point of lines equating to the x-axis, and y-axis, respectively. The transformation of this mesh structure is represented in Uddin and Nasrin (2023), There are n = 250 grid outlines measured separately and involved as lines, and concerning the marginal time point, the expression defines the value of a piece repetition of the loop. Assume, $\bar{T}''$, U'' and $\bar{C}''$ represent, $\bar{T}$, U, and $\bar{C}$, respectively, after a specific time interval.

Applying the EFDM in PDEs (10-14),

$$\frac{U'_{i,j}-U'_{i,j-1}}{\Delta X}+\frac{V'_{i,j}-V'_{i,j-1}}{\Delta Y}=0 \tag{18}$$

$$\frac{U''_{i,j}-U'_{i,j}}{\Delta\eta}+U'_{i,j}\frac{U'_{i,j}-U'_{i-1,j}}{\Delta X}+V'_{i,j}\frac{U'_{i,j+1}-U'_{i,j}}{\Delta Y}$$
$$=\frac{U'_{i,j+1}-2U'_{i,j}+U'_{i,j-1}}{(\Delta Y)^2}+Gr\bar{T}'_{i,j}+Gm\bar{C}'_{i,j}-MU'_{i,j}-NU'_{i,j}$$
$$\Rightarrow U''_{i,j}=U'_{i,j}+\Delta\eta\left(-U'_{i,j}\frac{U'_{i,j}-U'_{i-1,j}}{\Delta X}-V'_{i,j}\frac{U'_{i,j+1}-U'_{i,j}}{\Delta Y}\right.$$
$$\left.+\frac{U'_{i,j+1}-2U'_{i,j}+U'_{i,j-1}}{(\Delta Y)^2}+Gr\bar{T}'_{i,j}+Gm\bar{C}'_{i,j}-MU'_{i,j}-NU'_{i,j}\right) \tag{19}$$

$$\frac{\bar{T}'_{i,j}-\bar{T}_{i,j}}{\Delta\eta}+U'_{i,j}\frac{\bar{T}'_{i,j}-\bar{T}'_{i-1,j}}{\Delta X}+V'_{i,j}\frac{\bar{T}'_{i,j+1}-\bar{T}'_{i,j}}{\Delta Y}$$
$$=\frac{1}{Pr}\frac{\bar{T}'_{i,j+1}-2\bar{T}'_{i,j}+\bar{T}'_{i,j-1}}{(\Delta Y)^2}+Ec\left(\frac{U'_{i,j+1}-U'_{i,j}}{\Delta Y}\right)^2+R\frac{\bar{T}'_{i,j+1}-2\bar{T}'_{i,j}+\bar{T}'_{i,j-1}}{(\Delta Y)^2}+H\bar{T}'_{ij}$$

$$\Rightarrow \bar{T}''_{i,j}=\bar{T}'_{i,j}+\Delta\eta\left(-U'_{I,J}\frac{\bar{T}'_{i,j}-\bar{T}'_{i-1,j}}{\Delta X}-V'_{i,j}\frac{\bar{T}'_{i,j+1}-\bar{T}'_{i,j}}{\Delta Y}+\frac{1}{Pr}\frac{\bar{T}'_{i,j+1}-2\bar{T}'_{i,j}+\bar{T}'_{i,j-1}}{(\Delta Y)^2}+Ec\left(\frac{U'_{i,j+1}-U'_{i,j}}{\Delta Y}\right)^2\right.$$
$$\left.+R\frac{\bar{T}'_{i,j+1}-2\bar{T}'_{i,j}+\bar{T}'_{i,j-1}}{(\Delta Y)^2}+H\bar{T}'_{ij}\right) \tag{20}$$

$$\frac{\bar{C}''_{i,j}-\bar{C}'_{i,j}}{\Delta\eta}+U'_{i,j}\frac{\bar{C}'_{i,j}-\bar{C}'_{i-1,j}}{\Delta X}+V'_{i,j}\frac{\bar{C}'_{i,j+1}-\bar{C}'_{i,j}}{\Delta Y}=\frac{1}{Sc}\frac{\bar{C}'_{i,j+1}-\bar{C}'_{i,j}+\bar{C}'_{i,j-1}}{(\Delta Y)^2}$$

$$\Rightarrow \bar{C}''_{i,j}=\bar{C}'_{i,j}+\Delta\eta\left(-U'_{i,j}\frac{\bar{C}'_{i,j}-\bar{C}'_{i-1,j}}{\Delta X}-V'_{i,j}\frac{\bar{C}'_{i,j+1}-\bar{C}'_{i,j}}{\Delta Y}+\frac{1}{Sc}\frac{\bar{C}'_{i,j+1}-\bar{C}'_{i,j}+\bar{C}'_{i,j-1}}{(\Delta Y)^2}\right) \tag{21}$$

With BCs:

$$U^n_{i,0}=1,\ V^n_{i,0}=0,\ \bar{T}^n_{i,0}=1\ \bar{C}^n_{i,0}=1,\ U^n_{i,L}=0,\ \bar{T}^n_{i,L}=0,\ \bar{C}^n_{i,L}=0 \tag{22}$$

Where *i*, j, and L represent the grids characterized by their respective coordinates.

4.1 Convergence checking

Stability and convergence assessment are essential techniques before moving on to precise calculations. Therefore, it suggests that our computations can be relied upon and are trustworthy. According to Alam et al. (2006), Tarammim et al. (2020), Ullah et al. (2021), Jahir and Nasrin (2022), the generic formulas of the Fourier calculation for U',θ',φ' an infinitely extended duration, about, $\eta=0$ are $e_1^{i\bar{\alpha}\bar{x}}$ and $e_1^{i\bar{\beta}\bar{y}}$, where $i=\sqrt{-1}$.

Then
$$U':\Psi'(\eta)\,e_1^{i\bar{\alpha}\bar{x}}\,e_1^{i\bar{\beta}\bar{y}}$$
$$\bar{T}':\theta'(\eta)\,e_1^{i\bar{\alpha}\bar{x}}\,e_1^{i\bar{\beta}\bar{y}} \tag{23}$$
$$\bar{C}':\varphi'(\eta)\,e_1^{i\bar{\alpha}\bar{x}}\,e_1^{i\bar{\beta}\bar{y}}$$

And following the time phase is acquired:

$$\begin{aligned} U' &: \Psi''(\eta)\, e_1^{\,i\bar{\alpha}\bar{x}}\, e_1^{\,i\bar{\beta}\bar{y}} \\ \bar{T}' &: \theta''(\eta)\, e_1^{\,i\bar{\alpha}\bar{x}}\, e_1^{\,i\bar{\beta}\bar{y}} \\ \bar{C}' &: \varphi''(\eta)\, e_1^{\,i\bar{\alpha}\bar{x}}\, e_1^{\,i\bar{\beta}\bar{y}} \end{aligned} \tag{24}$$

Putting equations (23) and (24) into equations (19) - (21), we get the following criteria. The specifics of the computation are provided in Uddin and Nasrin (2023).
The convergence constraints for EFDM-solving techniques are as follows:

$$\begin{aligned} &1-2a_1-2b_1-4c_1-2c_1Ec \le -1. \\ &2\left(a_1+b_1+2c_1+c_1Ec\right) \le 2. \\ &a_1+b_1+2c_1+c_1Ec \le 1. \\ &\frac{U'\Delta\eta}{\Delta X}+\frac{|V'|\Delta\eta}{\Delta Y}+\frac{2\Delta\eta}{(\Delta Y)^2}+\frac{\Delta\eta}{(\Delta Y)^2}Ec \le 1. \end{aligned} \tag{25}$$

Likewise, the second condition: $\frac{U'\Delta\eta}{\Delta X}+\frac{|V'|\Delta\eta}{\Delta Y}+\frac{1}{Pr}\frac{2\Delta\eta}{(\Delta Y)^2}+R\frac{2\Delta\eta}{(\Delta Y)^2} \le 1.$ (26)

The third condition: $\frac{U'\Delta\eta}{\Delta X}+\frac{|V'|\Delta\eta}{\Delta Y}+\frac{1}{Sc}\frac{2\Delta\eta}{(\Delta Y)^2} \le 1.$ (27)

The values $\Delta\eta = 0.005$, $\Delta x = 0.4$ and $\Delta y = 0.1$, along with the primary conditions establishing the method's convergence specifications, are $Pr \ge 1$ and $Sc \ge 0.22$ with physically consistent restraints. The central processing unit (CPU) average time to get the convergent solution is 1200 s.

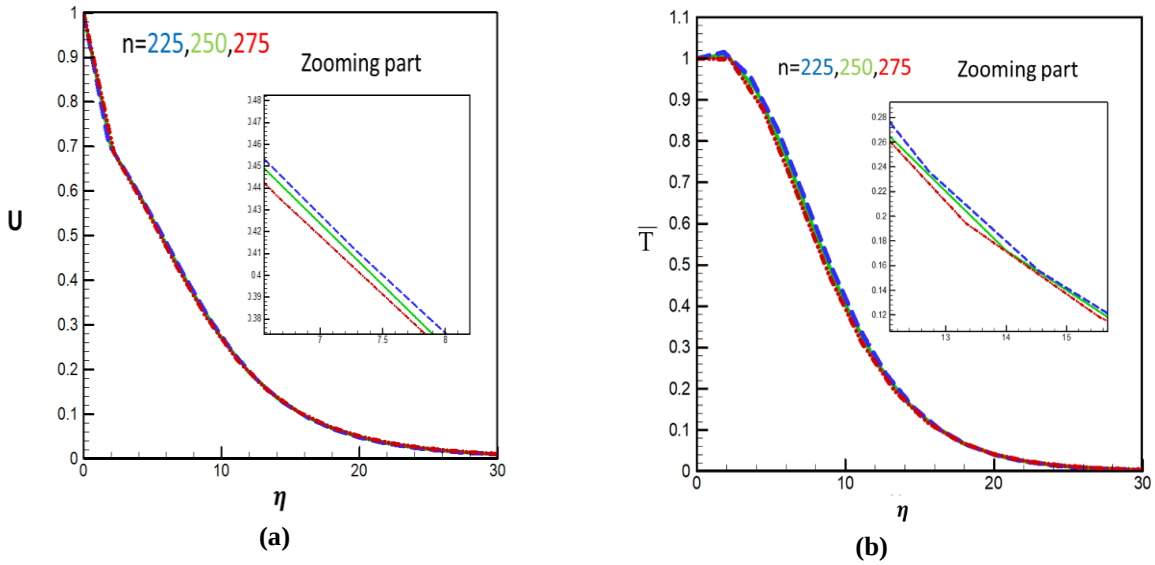

Figure 2: Grid-independence checking for (a) velocity and (b) thermal fields.

4.2 Grid-independence checking

The most suitable grid point for modeling fluid flow inside the BL flow area is determined through sequential testing of various grid points. Three strategically important experimental values are n = 225, n = 250, and n = 275. The technique is evaluated in an experiment and contrasted with the hypothesis of the subsequent trial. Figures 2(a) and 2(b) graphically illustrate the outcomes of this experiment for the influence of the magnetic factor on flow and thermal with different parameters. A thorough understanding of the consistency and

convergence of the graphs mains to the inference that the grid point n = 250 is the estimated choice for numerical configurations.

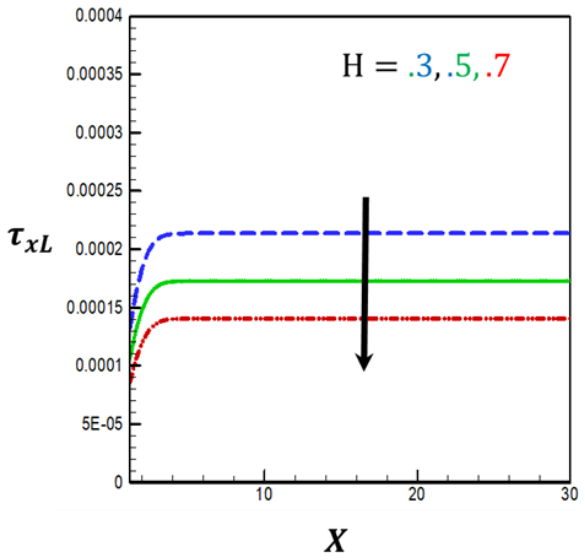

Figure 3: Stable-state situation of local shear stress due to heat generation at Y = 0.2, 0.4, 1, and 2.

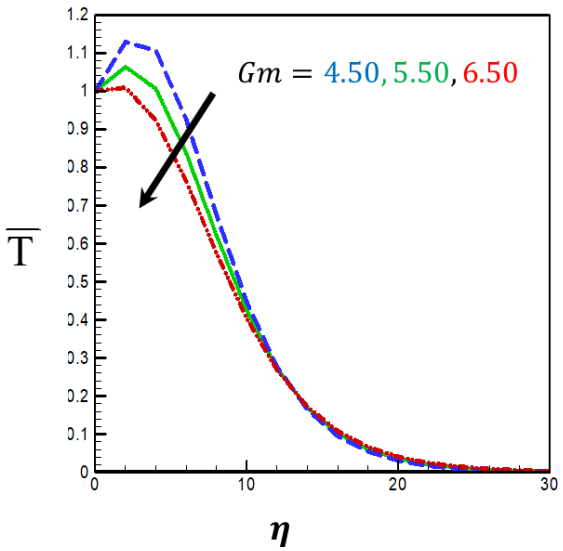

Figure 4: Temperature distribution due to solutal Grashof number variation compared with Figure 5.4 of Otieno et al. (2017)

4.3 Steady-state checking

The stable-state condition for the stream mathematical model is achieved by constantly analyzing different parameter values. The stable-state parameters for heat generation on shear stress at Y = 0.2, 0.4, 1, and 2 are shown in Figure 3 through M = 9.5, Sc = 0.22, Gr = 3.5, H = 0.3, Gm = 4.5, Pr = 1, R = 1, N = 1, and Ec = 0.1. The findings indicate that the significance of heat production on shear stress fluctuates minimally at Y = 0.2 and 0.4. As an acquirable stable state for the revealing fields, Y = 1 and Y = 2 exhibit almost insignificant variations. The stable-state presentation is shown in Figure 3 (Table 1).

Table 1: Stable state for heat generation on shear stress going to Figure 5 at Y = 0.2, 0.4, 1, and 2.

Average skin friction						
Generating heat (H)	Unstable		Oscillation (Unstable)%	Stable-state		Oscillation (Unstable)%
	Y = 0.2	Y = 0.4		Y = 1	Y = 2	
H = 0.3	0.000184	0.000213	2.91721E-05	0.000213	0.000213	0
H = 0.5	0.000148	0.000172	2.41252E-05	0.000172	0.000172	0
H = 0.7	0.000105	0.000140	3.43296E-05	0.000140	0.000140	0

4.4 EFDM coding validation

The reported finding of Otieno et al. (2017) and the present result demonstrate an outstanding potential. Otieno et al. (2017) scrutinized the mathematical calculation of magneto-convective heat and mass transmission across an infinitely inclined sheet with buoyancy forces. Figure 4 in this research and Figure 5.4 from Otieno et al. (2017) illustrate the outcomes of the picture-to-picture comparison. This contrast investigates the impression of the mass Grashof number (Gm) on the temperature distributions within the BL.

The exemplary equations above are mathematically simulated exhausting LAHEY FORTRAN 95 v 6.2. Tecplot 7.0 and Microsoft Excel 19 are utilized for data analysis and visual representation. The combination of simplicity, computational efficiency, adaptability, and flexibility makes EFDM a valuable tool for foundational studies and novel research in fluid dynamics such as case studies, benchmarking, novel flow configurations, and parametric studies.

Our current numerical study has not encountered any dual or multiple solutions. We perform essential checks, including convergence, grid independence, and stability assessments, and confirm unique solutions for all dependent variables, including velocity components, pressure, temperature, and concentration. Furthermore, we validate our EFDM coding to ensure the robustness of our numerical code for conducting boundary layer flow analyses.

5. Outcomes

The movement of heat and materials is driven by buoyant forces caused by temperature and solute concentration changes. The study focuses on heat and mass transfer involving water as a liquid and hydrogen as a gas. With a Prandtl number (*Pr*) of 1 for water and a Schmidt number (*Sc*) of 0.22 for hydrogen, it addresses the relationship between momentum and mass transfer in these phases. Additionally, the research explores MHD and heat transfer, suggesting the presence of electrically conductive fluids, such as water or electrolyte solutions, under magnetic field influence. To obtain a comprehensive understanding of the research, extensive calculations are conducted to assess the effects of hydrodynamic and thermofluidic variables on the dimensionless velocity, thermal, and concentration properties, along with the local and mean Sherwood number, Nusselt number, and skin-friction coefficients. These numerical outcomes are depicted in Figures 5-7. In our current numerical study, we are specifically focusing on heat generation (*H*) values of 0.3, 0.5, and 0.7, thermal Grashof number (*Gr*) values of 3.5, 4.5, and 5.5, and solutal Grashof number (*Gm*) values of 4.5, 5.5, and 6.5. Based on (Ajay and Srinivasa, 2021, Arifuzzaman et al. 2018, Krishna et al. 2019. Hossain, et al. 2023). research, these values are carefully selected for mathematical simulation. Heat generation within the boundary layer depends on internal heat sources such as chemical reactions, electrical heating, radiation, and thermal-solute buoyancy forces acting on the fluid. Using these values of *H*, *Gr*, and *Gm* is crucial for accurate mathematical simulations and appropriate graphical representations. Utilizing higher values may lead to undesired outputs. For mathematical and numerical calculations, the subsequent defaulting factor values are used magnetic field, M = 9.5, Schmidt number, Sc = 0.22, Prandtl number, *Pr* = 1, thermal radiation, R = 1, Eckert number, *Ec* = 0.1, and porosity, *N* = 1. These values signify the predominant conduction of the respective chemical species. The Prandtl number is calculated using typical numerical values, such as 1 for water at 4°C, representing the water as the heat-transferring fluid.

5.1 Influence of thermal Grashof number (*Gr*)

The thermal Grashof number (*Gr*) is a dimensionless indicator that quantifies the balance of buoyancy and viscous forces within a fluid flow. This parameter holds significance in natural convection phenomena, where temperature differentials trigger variations in density, driving flow through buoyancy forces. A high thermal Grashof number amplifies fluid velocity and heat transfer by bolstering buoyancy forces, producing more pronounced temperature gradients, and promoting uniform concentration profiles. Figure 5(a-k) illustrates the influence of thermal *Gr* on the BL flow in the following circumstances: *M* = 09.5, *Pr* = 01.0, *Gm* = 04.5, H = 00.3, Sc = 0.22, *Ec* = 00.1, *N* = 01.0, and *R* = 01.0. Figures 5(a)-(c) elucidate the significance of the buoyancy force factor on flow, thermal, and mass distribution. Figure 5(a) It is perceived that the fluid velocity grew as Gr raised, resulting in an upsurge in velocity as a consequence of the thermal buoyancy force (buoyancy-assisted force), which generates a pressure gradient (Table 2). Because the heat transmission specifies the proportion of the thermal buoyant force to the viscous force. Physically, raising the Gr decreases the viscous and thermal buoyancy forces, resulting in a rise in flow distribution. Figure 5(b) demonstrates that as the value of *Gr* rises, the thermal drops (Table 3). This means that with an upsurge in results, the rate of thermal falls inside the BL, and as a result, higher rates of heat mass transfer drop. The mass profile declines for growing prescribed values in Figure 5(c). The growing importance of lowering the thermal buoyancy influence; decreases the heat and mass transmission rate (Table 4). So, the rushing of fluid velocity is correlated with a lessening in the thickness of the thermal material BL for higher temperature and concentration gradients. Figures 5(d) and 5(g) demonstrate Nu_L and Nu_A increases for growing values of *Gr*.

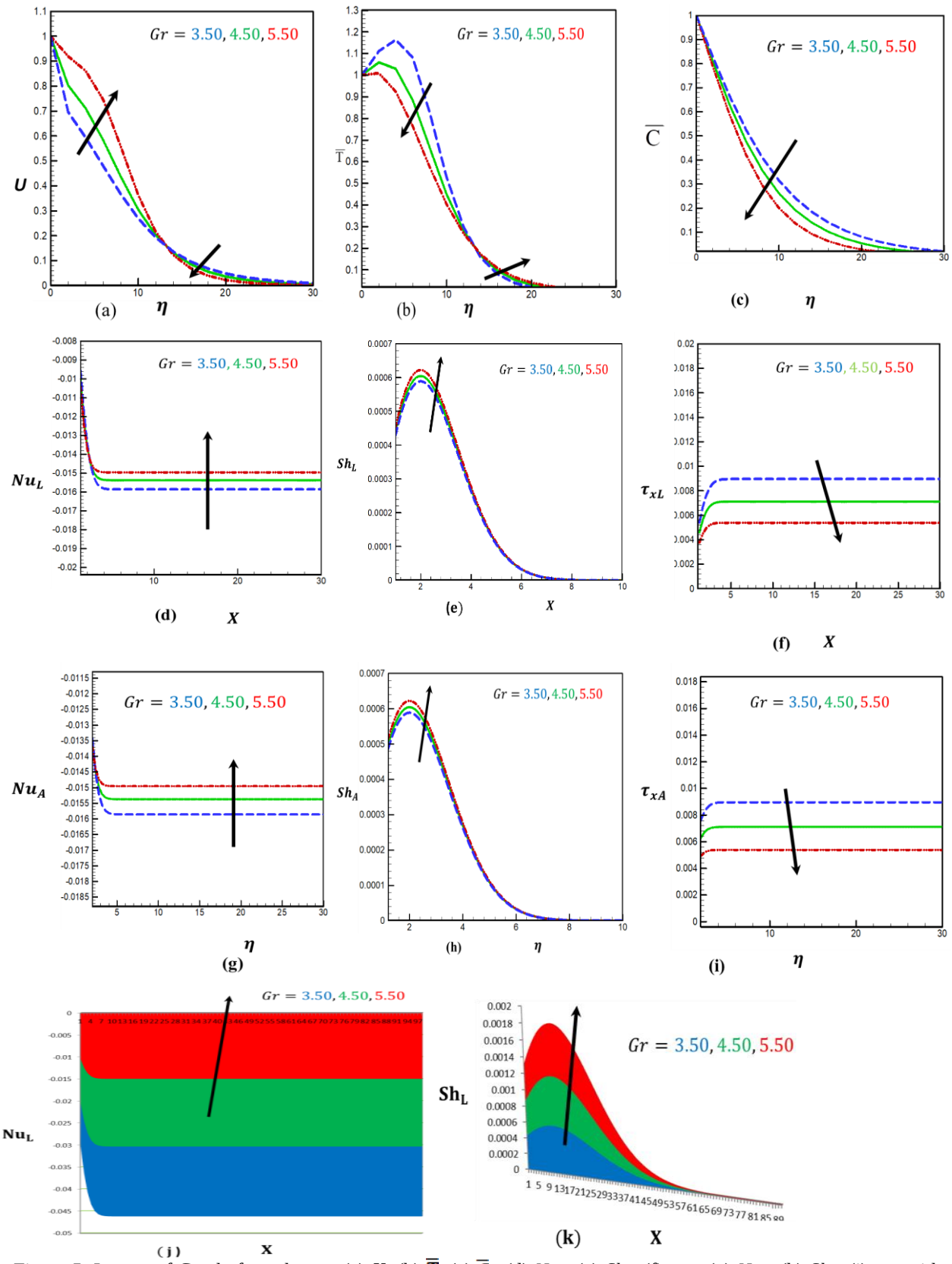

Figure 5: Impact of Grashof number on (a) $\boldsymbol{U}$, (b) $\overline{\boldsymbol{T}}$, (c) $\overline{\boldsymbol{C}}$, (d) Nu_L, (e) Sh_L, (f) $\boldsymbol{\tau_{xL}}$, (g) Nu_A, (h) Sh_A, (i) $\boldsymbol{\tau_{xA}}$ with (j) Nu_L, (k) Sh_L in 3D structure.

It is the occurrence that rising value stands to intensify the buoyancy effect. It contributes to the upsurge in the influenced flow. The influence of the *Gr* on Sh_L and Sh_A are observed in Figs 5(e) and 5(h); this result shows Sh_L and Sh_A rises for increasing values of *Gr*. The increasing thickness of the boundary layer reduces the local and average mass transfer coefficient, as species diffusion across the thicker layer is less efficient than a thinner boundary layer. Figs 5(f) and 5(i) demonstrate τ_{xL} and τ_{xA} decline for enhancement of *Gr*. It becomes apparent that the transient velocity upsurges due to a rise in the thermal buoyancy effect.

Table 2: Line-to-line variability for Figure 5(a) at $Y = 1$.

Velocity		
Thermal Grashof Number (*Gr*)	Numeric Value	Increase/Decrease (%)
3.5	0.269696	
4.5	0.304965	3.526917% increase
5.5	0.363196	5.823106% increase

Table 3: Line-to-line variability for Figure 5(b) at $Y = 1$.

Temperature		
Thermal Grashof Number (*Gr*)	Numeric Value	Increase/Decrease (%)
3.5	0.527471	
4.5	0.448593	7.887763% decrease
5.5	0.402988	4.560545% decrease

Table 4: Line-to-line variability for Figure 5(c) at $Y = 1$.

Concentration		
hermal Grashof Number (*Gr*)	Numeric Value	Increase/Decrease (%)
3.5	0.314717	
4.5	0.261336	5.338112% decrease
5.5	0.200201	6.113547% decreas

5.2 Influence of solutal Grashof number (*Gm*)

The solutal Grashof number (*Gm*) is a dimensionless parameter used to quantify the relative importance of buoyancy forces caused by variations in solute concentration compared to viscous forces in a fluid flow. It is a dimensionless quantity that describes the impact of concentration gradients on fluid motion.When its value is high, it leads to stronger buoyancy forces due to concentration differences, enhancing fluid velocity and solute mixing. This results in more uniform concentration profiles and indirectly affects the temperature profile by improving convective heat transfer. It is especially significant in scenarios where the flow is driven by differences in solute concentration instead of temperature gradients. A variety of physical events, including thermal and mass buoyancy forces may influence the motion of fluid flow (solutal Grashof number) which is shown in figure 6(a-j) at M = 09.5, Sc = 0.22, Gr = 03.5, H = 0.3, Pr = 01.0, N = 01.0, $Ec =$ 0.1, and R = 01.0. Figure 6(a) demonstrates the flow distribution upsurges for rising values of *Gm* owing to the mass buoyancy force. The *Gm* determines the ratio between the buoyancy force of the species and its hydrodynamic viscosity. Realistically, the fluid velocity rises substantially when the buoyancy force of a species grows. The fluid stream rate reaches the definite highest point near the sheet surface, steadily declining until it refers to the free stream's value. It is found in Figure 6(b) that the thermal distribution falls for growing deals *Gm*. In actuality, mass buoyancy forces decay the heat transmission. The material distribution decreases when *Gm* values increase as shown in Figure 6(c). Mass Grashof number is the species' buoyancy force ratio to the viscid hydrodynamic force**.** The growing importance of the *Gm* declines the heat transmission rate. Subsequently, Nu_L and Nu_A fall, which are shown in Figures 6(d) and 6(g) (Table 5, and Table 6). Increasing values of *Gm* can enhance local and average heat transfer, it leads to improved mixing and reduced thermal resistance.

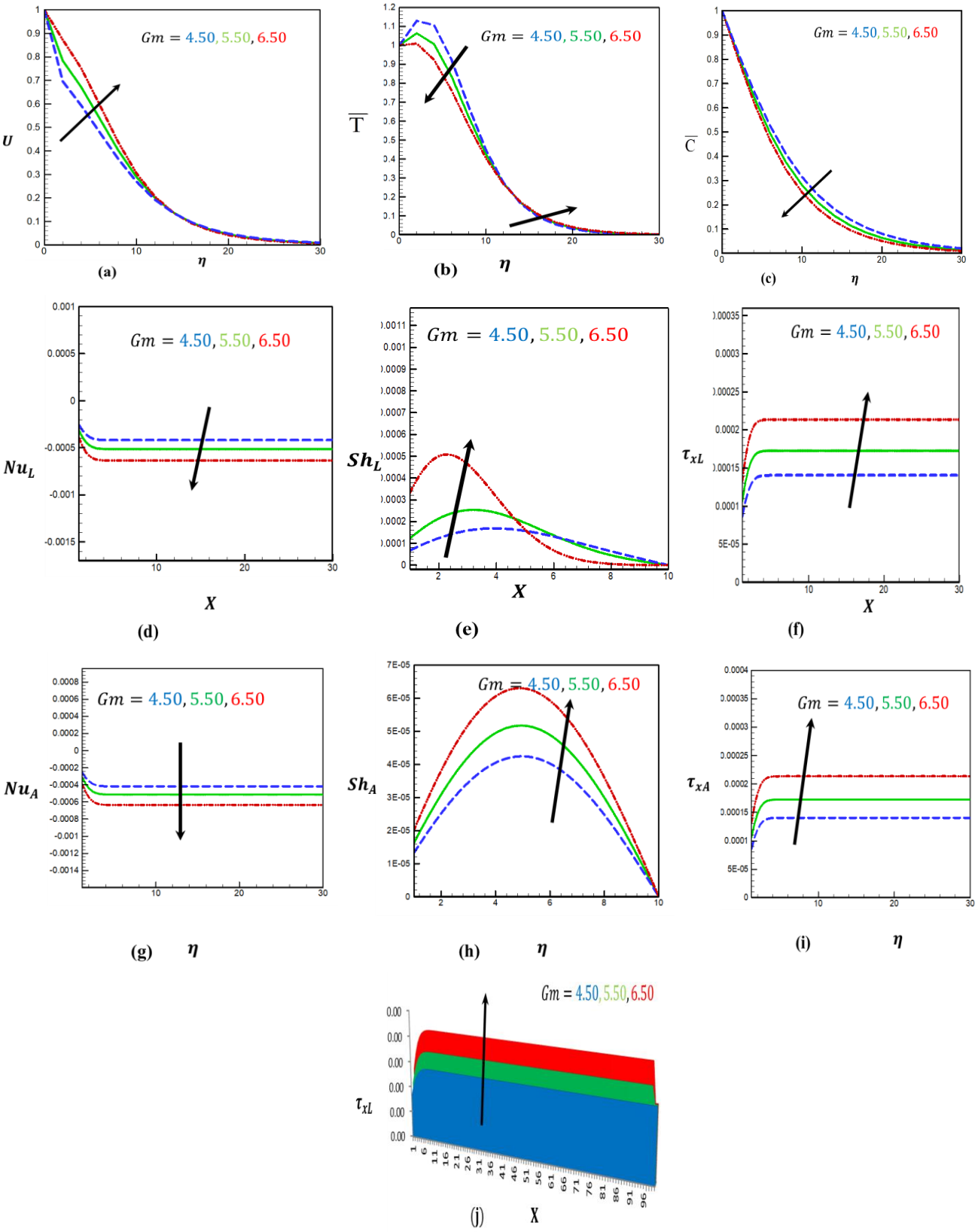

Figure 6: Impact of modified Grashof number on (a) $\boldsymbol{U}$, (b) $\overline{\boldsymbol{T}}$, (c) $\overline{\boldsymbol{C}}$ (d) $\boldsymbol{Nu_L}$, (e) $\boldsymbol{Sh_L}$, (f) $\boldsymbol{\tau_{xL}}$, (g) $\boldsymbol{Nu_A}$, (h) $\boldsymbol{Sh_A}$, (i) $\boldsymbol{\tau_{xA}}$, (j) τ_{xL} in three dimension structure

The influence of *Gm* on Sh_L and Sh_A are observed in figures 6(e) and 6(h). This result shows that $Sh_L$and Sh_A upsurge with growing *Gm* values. As projected, the Gm inclines to upsurge mass buoyancy force. Consequently, the rate of stream of the fluid rises. Figures 6(f) and 6(i) exhibit τ_{xL} and upsurges for growing values of *Gm* owing to the mass buoyancy force. Due to this, the mass transmission increases skin friction.

Table 5: Line-to-line variability for Figure 6(d) at $Y = 1$.

Local Nusselt number		
Solutal Grashof number (Gm)	Numeric Value	Increase/Decrease (%)
4.5	-0.000634	
5.5	-0.000513	0.012150% decrease
6.5	-0.000417	0.009544% decrease

Table 6: Line-to-line variability for Figure 6(g) at $Y = 1$.

Average Nusselt number		
Solutal Grashof number (Gm)	Numeric Value	Increase/Decrease (%)
4.5	-0.014953	
5.5	-0.000513	1.444039% decrease
6.5	-0.000417	0.009544% decrease

5.3 Influence of heat generation (H)

The internal heat generation parameter (H) measures how much heat is generated within the fluid. When H has a high value, it increases fluid velocities due to stronger buoyancy effects. This, in turn, creates higher temperature gradients near the surface. A high value of H also leads to more uniform concentration profiles in the fluid due to improved diffusion and mixing processes. This parameter notably impacts dimensionless parameters such as the local and mean Nusselt number, the local and mean Sherwood number, and the local and mean skin friction coefficient. Specifically, higher values of H result in increased Nusselt and Sherwood numbers, along with higher skin friction. These effects are attributed to enhanced heat and mass transfer rates and higher shear stress from improved fluid motion. Figures 7(a) and 7(d) demonstrate that Nu_L and Nu_A decrease for growing values of temperature generation (Table 7, and Table 8). It may be explained by the tendency to produce heat to reduce stream temperature. Thereby diminishing the thermal buoyancy force and causing a net decline in fluid temperature. The effect of H on Sh_L and Sh_A are observed in Figures 7(b) and 7(e) (Table 9); this result shows that Sh_L and Sh_A declines for enhanced thermal generation. The concentration gradient at the surface is lessened due to the thicker thermally boundary layer. Figures 7(c) and 7(f) demonstrate τ_{xL} and τ_{xA} decline for enhancement of H (Table 10, and Table 11). It is shown that higher heat production results in a thinner boundary layer and an inferior velocity field. This deteriorating trend points to the physical situation of the suction impact, which is that it delays the process of separation and transfer and assists in maintaining the constant flow of the sheet.

Table 7: Line-to-line variability for Figure 7(a) at $Y = 1$.

Local Nusselt number		
Heat Generation (H)	Numeric Value	Increase/Decrease (%)
0.3	-0.000634	
0.5	-0.000513	0.060751% decrease
0.7	-0.000417	0.047718% decrease

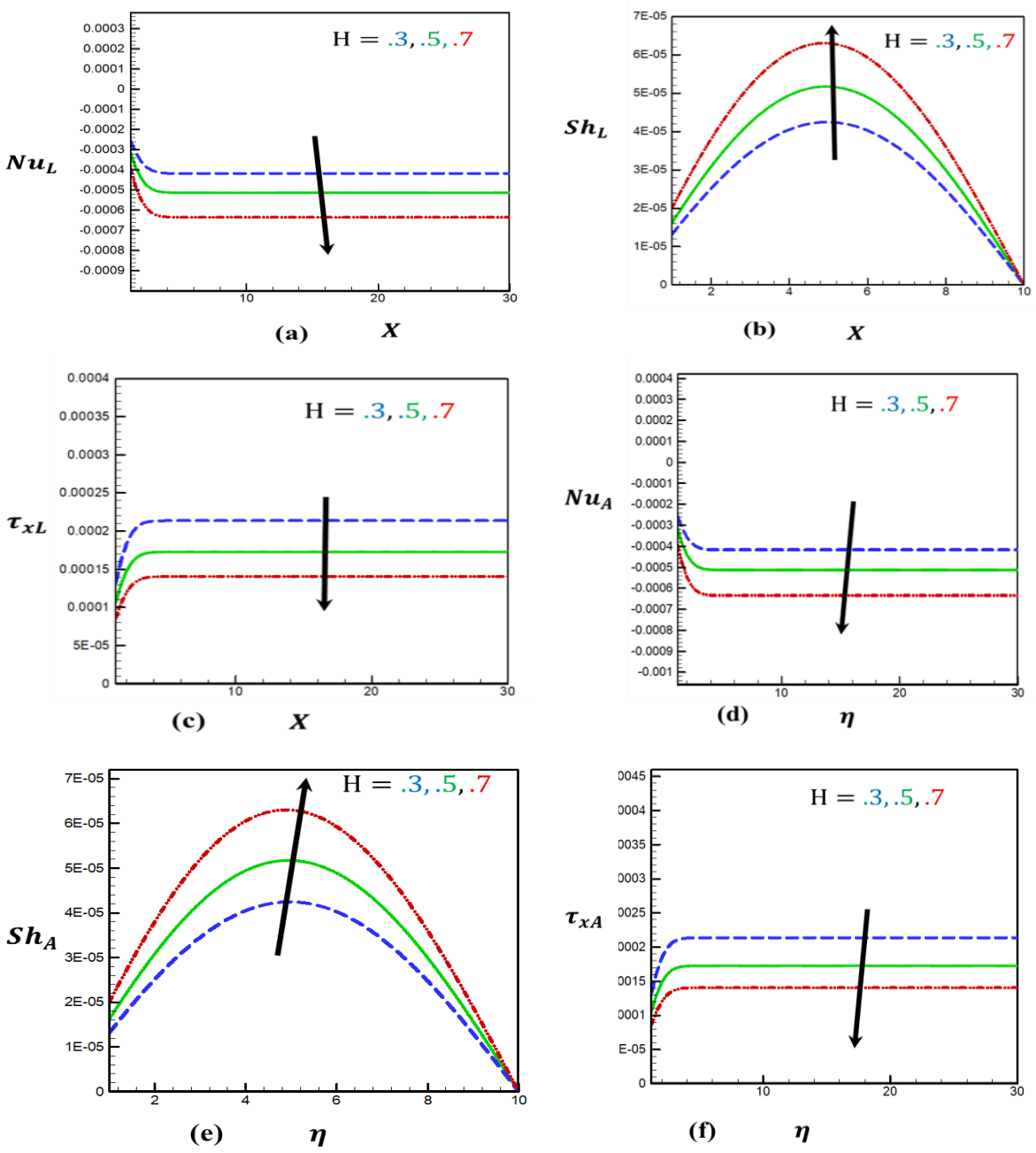

Figure 7: Impact of heat generation on (a) Nu_L, (b) Sh_L through M = 9.5, Gm = 4.5, Sc = 0.22, Gr = 3.5, Ec = 0.1, Pr = 1, N = 1, and R = 1., (c) τ_{xL}, (d) Nu_A, (e) Sh_A (f) τ_{xA} through M = 9.5, Gm = 4.5, Sc = 0.22, Gr = 3.5, Ec = 0.1, Pr = 1, N = 1, and R = 1.

Table 8: Line-to-line variability for Figure 7(d) at Y = 1.

Average Nusselt number		
Heat Generation (H)	Numeric Value	Increase/Decrease (%)
0.3	-0.000634	
0.5	-0.000513	0.060751% decrease
0.7	-0.000417	0.047718% decrease

Table 9: Line-to-line variability for Figure 7(b) at $Y = 0.5$.

Local Sherwood number		
-Heat Generation (H)	Numeric Value	Increase/Decrease (%)
0.3	0.000062	
0.5	0.000052	0.005285% increase
0.7	0.000042	0.004621% increase

Table 10: Line-to-line variability for Figure 7(c) at $Y = 1$.

Local Skin friction		
Heat Generation (H)	Numeric Value	Increase/Decrease (%)
0.3	0.000214	
0.5	0.000173	0.020500% decrease
0.7	0.000140	0.016083% decrease

Table 11: Line-to-line variability for Figure 7(f) at $Y = 1$.

Average Skin friction		
Heat Generation (H)	Numeric Value	Increase/Decrease (%)
0.3	0.000062	
0.5	0.000052	0.005620% decrease
0.7	0.000042	0.004621% decrease

5.4 Comparison

The Nu_L influences the expansion of the heat stream at any position, and the Nu_A matters at every location. Consequently, the Nu_A, equals the Nu_Lunder these conditions due to a combination of aspects. The Sh_L influences the growth of material transfer at any given point, and the Sh_A is significant at all locations. Therefore, the Sh_A is identical to the Sh_L for various factors. In these instances, the parameters affect τ_{xL}. The subsequent table (Table 12) provides a qualitative assessment of the reported study and that of various researchers from previous studies.

This research aims to find the numerical solution for magnetron-convective flow, which is viscid, electrically accompanying, viscoelastic, radiating fluid flows about a spongy sheet. Reddy et al. (2018) scrutinized the implications of radiative heat flux, and heat production on MHD convective thermal flux about an inclined porous sheet with a chemical reaction. Alam et al. (2021) scrutinized the MHD fluid stream about an incline impervious flat sheet with thermal and radiative heat fluxes. They use EFDM for numerical solutions. Javaherdeh et al. (2015) analyzed magneto-convective fluid stream about an upright permeable sheet with inconstant apparent material and thermal distribution.

Table 12: Comparing present results to previously reported outcomes.

	Reddy et al. (2018)			Alam et al. (2021)			Present results			
Parameters	*U*	*T*	Sh_L	*U*	*T*	*C*	*U*	*T*	*C*	Sh_L
Gr	Ups	Fal	Ups	Ups	Fal	Fal	Ups	Fal	Fal	Ups
Gm	Ups	Fal	Ups	Ups	Fal	Fal	Ups	Fal	Fal	Ups
	Javaherdeh et al. (2015)						Present results				
	U	*T*	*C*	Sh_L	Nu_L		*U*	*T*	*C*	Sh_L	Nu_L
Gr	Ups	Fal	Fal	Ups	Ups		Ups	Fal	Fal	Ups	Ups

Ups means Upsurge, and Fal means Fall.

5.5 Regression equation

A regression equation is crucial in data analysis because it can model relationships, predict outcomes, provide insights, and support decision-making. They are versatile tools capable of handling complex data, identifying key drivers, and optimizing processes, making them essential in academic research and practical applications.

The findings of this research have facilitated the derivation of two new multiple-variable linear regression equations for thermal-material transport, precisely the mean Nusselt number (*Nu*) and mean Sherwood number (*Sh*). These equations factor in the buoyancy force due to temperature difference (*Gr* = 3.5-5.5), buoyancy force due to material concentration difference (*Gm* = 4.5-6.5), and heat generation (*H* = 0.3-0.7). We use 27 observations for these derivations with a total degree of freedom of 26 (regression 3, residual 23).

The regression equation for *Nu* is:

$$Nu = -0.029164 + 6.08*10^{-4}Gr + 7.627*10^{-4}Gm + 3.656*10^{-2}H. \quad (28)$$

where the multiple R (correlation coefficient) is 0.8016, the adjusted R-squared is 0.5540, the R-square (R^2) value is 0.6516, the standard error is 0.00565, the total sum of square (SS) is $9.814*10^{-3}$, total mean of square (MS) is $11.42*10^{-4}$, F value is 0.2578 and the significance F (p-value) associated with this equation is $7.8341*10^{-3}$.

The regression equation for *Sh* is:

$$Sh = 0.000328 - 3.4*10^{-7}Gr - 1.5*10^{-5}Gm - 3.4*10^{-4}H. \quad (29)$$

Here the multiple R is 0.7932, the adjusted R-squared is 0.4445, the R^2 is 0.5432, the standard error is $5.39*10^{-4}$, SS is $8.82*10^{-7}$, MS is $10.05*10^{-8}$, F value is 0.2464 and significance F is $8.79*10^{-3}$.
The above-derived regression equations are statistically and enormously significant.

6. Concluding Remarks

The analysis focuses on the numerical outcomes of the magneto-convective radial thermal and material transmission flow of an electrically accompanying fluid, which shows thermal radiation. This flow occurs around an upright permeable flat sheet, under the impact of thermal and solute buoyancy forces. The analysis is based on previously generated tabular and graphical results. For the inconsistent results, the study focused on an EFDM-solving strategy involving time-domain consideration. It offers significant benefits in environmental, energy, aerospace, automotive, biomedical, computational, and educational domains. This analysis reveals some critical engineering-related findings:

- The fluid movement rises by 3.52% and 5.82% as thermal buoyancy force changes from 3.50 to 4.50 and 4.50 to 5.50 respectively. As mass buoyancy force varies from 4.50 to 5.50 and 5.50 to 6.50, the fluid movement also increases by 1.61% and 1.96%.
- As thermal buoyancy force changes from 3.50 to 4.50 and 4.50 to 5.50, the fluid temperature declines by 7.88% and 4.56%. Additionally, as the mass buoyancy force moves from 4.50 to 5.50 and 5.50 to 6.50, respectively, the fluid temperature drops by 2.11% and 2.26%
- The material distribution declines by 5.33% % and 6.11% for increasing thermal buoyancy force, moving 3.50 to 4.50 and 4.50 to 5.50, respectively. Moreover, as the mass buoyancy force increases from 4.50 to 5.50 and 5.50 to 6.50, respectively, the material distribution decreases by 3.34% and 2.96 %.
- As the solutal Grashof number increases, the local and average skin friction coefficients rise by 0.004% to around 0.007%. Conversely, as the thermal Grashof number and temperature generation increase, they decrease by 0.18% to 0.17% and by 0.020% to 0.016%, respectively.
- Due to the rising thermal buoyancy force and heat production values, the local and average heat transport rates rise by 0.012% to 0.009% and 0.06% to 0.04% respectively. In contrast, they fall by 1.444% to 0.009% with growing values of the solutal Grashof number.
- The local and average mass transmission rates produce an impact on the heat production (0.005% - 0.004%), thermal buoyancy force (0.006% -0.009%), and solutal buoyancy force (0.0027% -0.0024%) to increase the values of their pertinent characteristics.

Based on this research, it is advised that to attain the optimum heat transfer rate, the following flow-controlling variables should be set: thermal buoyancy force (*Gr* = 5.50), solutal buoyancy force (*Gm* = 4.50), and heat generation (*H* = 0.3). Likewise, the recommended settings for achieving the optimum mass transfer rate are *Gr* = 5.50, *Gm* = 6.50, and *H* = 0.7.

The above findings of the study relate to the existing literature by building on established concepts, introducing novel methodologies, and extending the practical applications of boundary-layer flow analysis. This research addresses gaps in the literature and provides new insights and tools that can be utilized in both academic and industrial settings, thereby advancing the field of fluid dynamics and heat transfer.

The research on augmenting thermal-material transport in boundary-layer flows over an upright sheet using an explicit finite difference approach offers significant advancements across multiple fields. The study's findings and methodologies have the potential to drive innovation and contribute to the sustainable development of various technologies and systems. It enables the development of more efficient, optimized, and innovative solutions in engineering, environmental management, aerospace, automotive industries, biomedical devices, and beyond.

6.1 Recommendation

Our studies focus on the numerical investigation of time-dependent MHD thermal flows and Material transmission about a perpendicular permeable sheet beneath the impact of thermal buoyancy forces. This research provides the following suggestions:

- Considering the Hall current affects the slanted sheet and upward sheet with the flow pattern of the wavy stream.
- Contemplating the impress of Hall current and heat generation on the permeable flat sheet.
- Contemplating the indicating trajectory with inclined sheets in electric and magnetic fields.
- Contemplating the magnetic field that rotates in conjunction with the radiative factor.

References

Abdullameed, M., Khan, I., Shafie, S. (2013): Closed from solutions for unsteady MHD flow in a porous medium with wall transpiration, J. of Porous Media, Vol. 16, pp. 79.

Ahmed, K.F.U., Nasrin, R., and Elias, Md. (2018): Natural convective flow in circular and arc cavities filled with water-Cu nanofluid: a comparative study, Journal of Naval Architecture and Marine Engineering, Vol. 15, pp. 37-52, https://doi.org/10.3329/jname.v15i1.33549.

Ajay, C.K. and Srinivasa, A.H. (2021): The effect of internal heat generation (absorption)and Prandtl number on MHD mixed convection flow from a vertical flat plate, Malaya Journal of Matematik, Vol. 9(1), pp. 1135-1140. https://doi.org/10.26637/MJM0901/0197

Alam, M.S., Ali, M. and Hossain, M.D. (2013): Heat and mass transfer in MHD free convection flow over an inclined plate with Hall current, International Journal of Engineering Science, Vol. 2, pp. 81-88.

Alam, M.S., Rahman, M.M., Samad, M.A. (2006): Numerical study of the combined free-forced convection and mass transfer flow past a vertical porous plate in a porous medium with heat generation and thermal diffusion, Nonlinear Analysis: Modeling and Control, Vol. 11, pp. 331-343,

Alam, N., Poddar, S., Karim, M.E., Hasan, M.S., Lorenzini, G. (2021): Transient MHD radiative fluid flow over an inclined porous plate with thermal and mass diffusion: An EFDM numerical approach, Mathematical Modelling of Engineering Problems, Vol. 8(5), pp. 739-749.https://doi.org/10.18280/mmep.080508,

Ali, M., Alim, M.A., Nasrin, R., Alam, M.S., Chowdhury, M.Z.U. (2017): Magnetohydrodynamic boundary layer nanofluid flow and heat transfer over a stretching surface, AIP Conference Proceedings, 1851, 020022, https://doi.org/10.1063/1.4984651.

Ali, M., Alim, M.A., Nasrin, R., Alam, M.S., Munshi, M.J.H. (2017): Similarity solution of unsteady MHD boundary layer flow and heat transfer past a moving wedge in a nanofluid using the Buongiorno model, Procedia Engineering, Vol. 194(C), pp. 407-413. https://doi.org/10.1016/j.proeng.2017.08.164.

Ali, M., Alim, M.A., Nasrin, R., and Alam, M.S. (2016): Study the effect of chemical reaction and variable viscosity on free convection MHD radiating flow over an inclined plate bounded by porous medium, AIP Conference Proceedings, 1754, 040009. https://doi.org/10.1063/1.4958369

Ali, M., Alim, M.A., Nasrin, R., and Alam, M.S. (2017): Numerical analysis of heat and mass transfer along a stretching wedge surface, Journal of Naval Architecture and Marine Engineering, Vol.14(2), pp.135-144, https://doi.org/10.3329/jname.v14i2.30633.

Ali, M., Nasrin, R., Alim, M.A. (2021): Analysis of boundary layer nanofluid flow over a stretching permeable wedge-shaped surface with magnetic effect, Journal of Naval Architecture and Marine Engineering, Vol. 18(1), pp. 11-24. http://dx.doi.org/10.3329/jname.v18i1.44458.

Ali, M., Nasrin, R., and Alim, M.A. (2023): Axisymmetric boundary layer slip flow with heat transfer over an exponentially stretching bullet-shaped object: A Numerical Assessment, Heliyon, Vol. 9(3), e13671. https://doi.org/10.1016/j.heliyon.2023.e13671

Alqahtani, A.M., Zeeshan; Khan; W., Smarandache; F., Becheikh; N. Alroobaea, R. (2024): Numerical solution of hybrid nanofluid and its stability over permeable wedge sheet with heat transfer analysis, in IEEE Access, Vol. 12, pp. 57633-57645, https://doi.org/10.1109/ACCESS.2024.3378513.

Arifuzzaman, S.M., Khan, M.S., Mehedi, M.F.U., Rana, B.M.J., Ahmmed, S.F. (2018): Chemically reactive and naturally convective high speed MHD fluid flow through an oscillatory vertical porous plate with heat and radiation absorption effect, Eng. Sci. Tech., An Int. J., Vol. 21(2), pp 215-228, https://doi.org/10.1016/j.jestch.2018.03.004

Das, S., Guchhait, S., Jana, R., and Makinde, O. (2016): Hall effects on an unsteady magneto-convection and radiative heat transfer past a porous plate, Alexandria Engineering Journal, vol. 55(2), pp. 1321–1331.

Ge-JiLe, H., Nazeer, M., Hussain, F., Khan, M.I., Saleem, A., Siddique, I., (2021): Two-phase flow of MHD Jeffrey fluid with the suspension of tiny metallic particles incorporated with viscous dissipation and porous medium, Advances in Mechanical Engineering, Vol. 13(3), https://doi.org/10.1177/16878140211005960

Hossain, Md. M., Hasanuzzaman, Md., Hossain, M.M.T. and Nasrin, R. (2023): Unsteady magneto-convective heat-mass transport by micropolar binary mixture passing a vertical permeable surface, Science and Technology Asia, Vol. 28(1), pp. 33-47. https://doi.org/10.14456/scitechasia.2023.4

Islam, T., Parveen, N. and Nasrin, R. (2022): Mathematical modeling of unsteady flow with uniform/non-uniform temperature and magnetic intensity in a half-moon shaped domain, Heliyon, Vol. 8(3), pp. e09015, https://doi.org/10.1016/j.heliyon.2022.e09015.

Javaherdeh, K., Nejad, M.M., and Moslemi, M. (2015): Natural convection heat and mass transfer in MHD fluid flow past a moving vertical plate with variable surface temperature and concentration in a porous medium, Ayandegan Institute of Higher Education, Tonekabon, Iran, Vol. 18(3), pp. 423-431. https://doi.org/10.1016/j.jestch.2015.03.001.

Khan, Z., Khan, W., Arko, Yagoub, A.S., Egami, R.H., and Garalleh, H.A.L. (2024): Numerical stability of magnetized Williamson nanofluid over a stretching/shrinking sheet with velocity and thermal slips effect. Numerical Heat Transfer, Part B: Fundamentals, 1–21. https://doi.org/10.1080/10407790.2024.2321483

Krishna, H., Bindu, P., Nalleboyina, and Gurrampati, V.R.R. (2019): Radiation and chemical reaction effects on the boundary layer MHD Casson fluid on a vertical plate embedded in the porous medium, International Journal of Mechanical Engineering and Technology, Vol. 10(11), pp. 1-12, http://www.iaeme.com/ijmet/issues.asp

Makinde, O.D. and Aziz, A. (2010): MHD mixed convection from a vertical plate embedded in a porous medium with convective boundary conditions, International Journal of Thermal Sciences, Vol. 49, pp. 1813-1820.

Mosharrof, M., Nasrin. R., Hasanuzzaman, M. (2022): Radiative and MHD effects on time-dependent thermal-material transfer by micropolar binary mixture, Advances in Mathematical Physics, Vol. 2022, 2224435, https://doi.org/10.1155/2022/2224435.

Nasrin, R. and Alim, M.A. (2009): Combined effects of viscous dissipation and temperature dependent thermal conductivity on MHD free convection flow with conduction and Joule heating along a vertical flat plate, Journal of Naval Architecture and Marine Engineering, Vol. 6(1), pp. 30-40, https://doi.org/10.3329/jname.v6i1.2648.

Nasrin, R. and Alim, M.A. (2009): MHD free convection flow along a vertical flat plate with thermal conductivity and viscosity depending on temperature, Journal of Naval Architecture and Marine Engineering, Vol. 6(2), pp. 72 – 83, https://doi.org/10.3329/jname.v6i2.4994.

Nasrin, R., Hasan, S., Alatawi, E.S. and Biswas, C. (2024) Water-propylene glycol mixture-based nanofluid flow within interconnected domain: An innovative way of thermal enhancement, Journal of Nanofluids, Vol. 13, https://doi.org/10.1166/jon.2024.2200.

Otieno, O.R., Manyonge, A.W., Bitok, J.K. (2017): Numerical computation of steady buoyancy driven MHD heat and mass transfer past an inclined infinite flat plate with sinusoidal surface boundary conditions, Applied Mathematical Sciences, Vol. 11(15), pp. 711-729, https://doi.org/10.12988/ams.2017.7127.

Reddy, M.G., Reddy, N.B., Reddy, B.R. (2009): Unsteady MHD convection heat and mass transfer flow a semi-infinite vertical porous plate with variable viscosity and thermal conductivity, International Journal of Applied Mathematics and Mechanics, Vol. 5, pp. 1-14,

Reddy, S.H., Raju, M.C., Reddy, C.P. (2018): Joule heating and radiation absorption effects on MHD convective and chemically reactive flow past a porous plate, Bulletin of Pure and Applied Sciences, Vol. 37E(1), pp. 117-136, https://doi.org/10.5958/2320 3226.2018.00013.9.

Rosseland, S. (1936): Theoretical Astrophysics, Oxford University, New York.

Samiulhaq, Sohail, A., Vieru, D., Khan, I., Shafie, S. (2014): Unsteady magnetohydrodynamic force convection flow of a second-grade fluid in a porous medium with ramped wall temperature, PLoS One, Vol. 9, pp. e88765
Shamshuddin, M., Ghaffari, A. and Usman, (2022): Radiative heat energy exploration on Casson-type nanoliquid induced by a convectively heated porous plate in conjunction with thermophoresis and Brownian movements, International Journal of Ambient Energy, Vol. 43(1), pp. 6329–6340, https://doi.org/10.1080/01430750.2021.2014960.
Sohail, M., El-Zahar, E.R., Mousa, A.A.A., Nazir, U., Althobaiti, S., Althobaiti, A., Shah, N.A., and Chung, J.D. (2022): Finite element analysis for ternary hybrid nanoparticles on thermal enhancement in Pseudo-plastic liquid through porous stretching sheet. Sci Rep 12, 9219, https://doi.org/10.1038/s41598-022-12857-3
Tarammim, A., Ullah, M. and Uddin, M. (2020): A study of two dimensional unsteady MHD free convection flow over a vertical plate, Open Journal of Fluid Dynamics, Vol. 10, pp. 342-355.
Uddin, M.J., Nasrin, R. (2022): Radiation and heat generation effects on magneto-convective fluid flow over a vertical porous plate, Proceedings of MARTEC, Bangladesh, SSRN, http://dx.doi.org/10.2139/ssrn.4444054.
Uddin, M.J., Nasrin, R. (2023): A numerical assessment of time-dependent magneto-convective thermal-material transfer over a vertical permeable plate, Journal of Applied Mathematics, Vol.1, pp.1-19. https://doi.org/10.1155/2023/9977857
Ullah, M., Tarammim, A. and Uddin, M. (2021): A study of two dimensional unsteady MHD free convection flow over a vertical plate in the presence of radiation, Open Journal of Fluid Dynamics, Vol. 11, pp. 20-33.
Yun-Jie, X., Nazeer, M., Hussain, F., Khan, M.I., Hameed, M.K., Shah, N.A., Chung, D. (2021): Electro-osmotic flow of biological fluid in divergent channel: drug therapy in compressed capillaries, Scientific Reports, Vol. 11(1), pp. 1 – 13. https://doi.org/10.1038/s41598-021-03087-0
Zeeshan, Khan M.S., Khan, I., Eldin, S.M., Hira (2023): Numerical solution of heat and mass transfer using Buongionro nanofluid model through a porous stretching sheet impact of variable magnetic, heat source, and temperature conductivity. Sci Prog. 6(3), 368504231201542. https://doi.org/10.1177/00368504231201542
Zeeshan, K. I., Eldin, S.M., Islam, S., Khan, M.U. (2023): Two-dimensional nanofluid flow impinging on a porous stretching sheet with nonlinear thermal radiation and slip effect at the boundary enclosing energy perspective. Sci Rep 13, 5459l, https://doi.org/10.1038/s41598-023-32650-0